Molecular Insight into Adsorption and Diffusion of Alkane Isomer Mixtures in Metal−Organic Frameworks

Ravichandar Babarao, Yew Hin Tong, and Jianwen Jiang*

Department of Chemical & Biomolecular Engineering, National University of Singapore, 117576 Singapore

Received: March 13, 2009; Revised Manuscript Received: May 22, 2009

Adsorption and diffusion of alkane isomer mixtures (C_4 and C_5) are investigated in catenated and noncatenated metal−organic frameworks (IRMOF-13, IRMOF-14, PCN-6, and PCN-6′) using molecular simulations. Competitive adsorption between isomers is observed, particularly at high pressures, at which a linear isomer shows a larger extent of adsorption due to configurational entropy. An inflection is found in the isotherm as a consequence of sequential adsorption in multiple favorable sites. Compared with the noncatenated counterparts, IRMOF-13 and PCN-6 have a greater loading at low pressures because of the constricted pores and stronger affinity with adsorbate. However, the reverse is true at high pressures due to the smaller pore volume. Catenated MOFs exhibit larger adsorption selectivity for alkane mixtures than the noncatenated counterparts. Adsorption selectivity in the four MOFs is comparable to that in carbon nanotube and silicalite, though adsorption capacity is lower in the latter. It is found that diffusivity of alkane in MOFs decreases with the degree of branching because a slender isomer diffuses faster. With the presence of constricted pores, diffusivity in catenated MOFs is smaller than that in noncatenated counterparts. In IRMOF-14 and IRMOF-13 diffusivity decreases monotonically, while it initially increases and then decreases in PCN-6′. The diffusion selectivity in catenated IRMOF-13 and PCN-6 is larger than that in noncatenated IRMOF-14 and PCN-6′. This work provides insightful microscopic mechanisms for the adsorption and diffusion of alkane isomers in MOFs and reveals that both adsorption and diffusion selectivities can be enhanced by catenation.

1. Introduction

As a new family of hybrid nanoporous materials, metal−organic frameworks (MOFs) have attracted considerable interest in recent years.[1] Consisting of metal-oxide clusters and organic linkers, MOFs have high surface areas and well-defined pores.[2] More intriguingly, the pore sizes and volumes can be readily altered over a wide atomic-scale range by tailoring the metal-oxides and organic-linker.[3] As a consequence, MOFs provide a wealth of opportunities for engineering new functional materials with tunable properties and have been regarded as promising materials, particularly for gas storage and separation. Toward this end, a large number of experimental and simulation studies have been reported. For instance, MOFs with different organic groups were synthesized and used to assess CH_4 and CO_2 storage.[4,5] CH_4 adsorption was simulated in MOFs for the storage of an environmentally friendly energy source.[6] MOFs with various linkers, pore sizes, and topologies were investigated by simulation for CO_2 storage.[7,8] Using both experimental techniques and simulations, CO_2/CH_4 separation was studied in mixed-ligand MOFs, where mixture adsorption was predicted from single-component adsorption and subsequently verified by simulations.[9] Catenated MOFs were found to store H_2 more densely and possess a higher adsorption capacity than the noncatenated counterparts.[10,11] Separation of light gas mixtures in catenated MOFs was measured, and an enhanced selectivity was observed.[12] Adsorptive separation of CH_4/H_2 mixtures was simulated at room temperature, and the results showed a higher selectivity in catenated IRMOFs.[13]

Most reported studies for gas adsorption and separation in MOFs have focused on light gases. In chemical engineering processes and industrial applications, however, separation of alkane mixtures is crucial, e.g., after the catalytic cracking of alkanes in a petrochemical refinery. Numerous experimental and simulation studies have been carried out on alkane adsorption in a wide variety of adsorbents. For example, the enthalpies, Henry constants, van't Hoff pre-exponential factors, and separation factors of C_5-C_8 alkanes were determined in zeolites at 473−648 K. Both nonselective and selective adsorption were found between linear and branched alkanes depending on zeolite type.[14] The isosteric heats and adsorption isotherms of C_1, C_2, and C_3 alkanes were measured in high-silica zeolites, and an inverse relationship was observed between the limiting isosteric heat and pore diameter.[15] The adsorption capacities of linear C_6, C_7, C_8, and C_9 alkanes in microporous silica solids were measured at different temperatures, and the limiting adsorption energy was found to be more attractive for longer alkanes.[16] With the advanced configurational-bias Monte Carlo method, adsorption of nC_4 to nC_{12} was simulated in silicalite, and a linear dependence of isosteric heat on chain length was found.[17] The low-coverage sorption of normal alkanes from C_4 to C_{25} in silicalite, temperature-dependent configurations, and locations were examined.[18] The adsorption isotherms of C_1 to nC_5 were calculated in aluminophosphate $(AlPO_4)_5$, and surprisingly a low density−high density transition was observed resembling a capillary condensation.[19] Subtle entropy effects were investigated in the adsorption of multicomponent mixtures of linear and branched alkanes in silicalite, and the development of novel separation processes was demonstrated.[20,21] Adsorption of C_5 isomers in carbon nanotubes and nanoslits was studied by simulations. The length and area entropy effects were found to play a key role, and the pore size rather than pore geometry determines the shape and inverse-shape selective adsorption.[22−24]

* Corresponding author. Telephone: +65 65165083. Fax: +65 67791936. E-mail address: chejj@nus.edu.sg.

10.1021/jp902253p CCC: $40.75
Published on Web 06/17/2009

A few simulation and experimental studies of alkanes in MOFs occurred only recently. The adsorption of C_1 and nC_4 and their mixtures in IRMOFs was simulated, and the influence of the organic-linkers on adsorption and selectivity was analyzed.[25] A simulation study of pure and mixed linear and branched alkanes suggested that IRMOF-1 might be a good candidate for the storage and separation of hydrocarbons.[26] From a fixed-bed adsorption experiment, a microporous MOF with two types of intersecting pores was found to discriminate *n*-hexane from branched hexanes.[27] The chromatographic separation of alkane isomers based on size- and shape-selectivity was investigated in a microporous MOF-508.[28] Unique gas and hydrocarbon adsorption was measured experimentally in a highly porous MOF composed of extended aliphatic ligands, and a transition from monolayer adsorption to pore filling was observed upon increasing temperature.[29] The siting and segregation of complex alkane mixtures were simulated in MOF-1, which suggested new possibilities for the design and creation of highly selective adsorption sites in MOFs.[30] Alkanes in Cu-BTC were studied by infrared microscopy and simulation, and strong inflection characteristics were found in the isotherms due to the preferential locations close to the mouths of tetrahedral pockets.[31]

Currently, the intriguing properties of alkane isomers confined in MOFs remain elusive. For example, where are the preferential binding sites located in a framework? Why does competitive adsorption occur between isomers? How does framework topology come into play? In this work, we aim to address these important issues by investigating the adsorption and diffusion of C_4 and C_5 isomer mixtures in two types of MOFs, noncatenated (IRMOF-14 and PCN-6′) and catenated (IRMOF-13 and PCN-6). Catenation results in constricted pores and has the benefit of increasing surface-to-volume ratio and framework stability. Hydrogen sorption in PCN-6 and PCN-6′ revealed that catenation leads to a 41% improvement in surface area and a 133% increase in volumetric uptake (29% increase in gravimetric unit).[11] However, knowledge on the microscopic behavior of alkane isomers and their mixtures in catenated MOFs is lacking. In section 2, the models for alkanes and MOFs are described. The simulation methods for adsorption and diffusion are given in section 3, including Monte Carlo (MC) and molecular dynamics (MD) simulations. In section 4, adsorption isotherms and selectivities of C_4 and C_5 isomer mixtures are presented. The adsorption properties in MOFs are compared with those in carbon nanotube and silicalite. Diffusivities of C_4 and C_5 isomer mixtures are reported along with the corresponding mechanisms. Finally, the concluding remarks are summarized in section 5.

2. Models

Two types of models are commonly used to mimic alkane molecules, the united-atom model and the all-atom model.[32] Both models were found to give comparable adsorption isotherms for alkanes in silicalite; however, computation was faster with the united-atom model.[33] Consequently, in this work the united-atom model was used with every CH_x group as a single interaction site. The C−C bonds were assumed to be rigid and fixed at 1.54 Å. The nonbonded dispersive interaction between sites of different molecules or four sites apart within a molecule was modeled by the Lennard-Jones (LJ) potential

$$u_{LJ}(r) = 4\varepsilon[(\sigma/r)^{12} - (\sigma/r)^{6}] \quad (1)$$

TABLE 1: Force Field Parameters for Alkanes[34,35]

	site	σ (Å)	ε/k_B (K)
nonbonded LJ	CH_3	3.75	98.0
	CH_2	3.95	46.0
	CH	4.68	10.0
	C	6.40	0.5
bond	CH_x-CH_y	$r_0 = 1.54$ Å	
bending	$CH_x-CH_2-CH_y$		
	$CH_x-CH-CH_y$	$k_\theta/k_B = 62500$ K	
	CH_x-C-CH_y	$\theta_0 = 113.0°$	
torsion	$CH_x-CH_2-CH_2-CH_y$	$c_0/k_B = 0$, $c_1/k_B = 355.03$,	
		$c_2/k_B = -68.19$, $c_3/k_B = 791.32$	
	$CH_x-CH_2-CH-CH_y$	$c_0/k_B = -251.06$, $c_1/k_B = 428.73$	
		$c_2/k_B = -111.85$, $c_3/k_B = 441.27$	

The bond bending between three successive sites was modeled using a harmonic potential

$$u_{bending}(\theta) = 0.5k_\theta(\theta - \theta_0)^2 \quad (2)$$

The dihedral torsion between four successive sites was modeled using a cosine potential

$$u_{torsion}(\phi) = c_0 + c_1[1 + \cos\phi] + c_2[1 - \cos(2\phi)] + c_3[1 + \cos(3\phi)] \quad (3)$$

Table 1 gives the force field parameters for alkanes, in which the LJ parameters were optimized to reproduce the experimental vapor−liquid coexistence curves and critical properties of pure alkanes.[34,35] It is noteworthy that the development of more accurate force fields for alkanes should take into account adjacent gauche stabilization.[36,37]

Figure 1 shows the atomic structures of four MOFs (IRMOF-14, IRMOF-13, PCN-6′, and PCN-6) examined under this study. IRMOF-14 has a cubic structure with a lattice constant of 34.38 Å.[4] It is formed by substituting 1,4-benzenedicarboxylate (BDC) in the prototype IRMOF-1 with pyrene-dicarboxylate (PDC), which is longer in length and leads to larger pores. The pore diameters in IRMOF-14 are approximately 20.1 and 14.7 Å. IRMOF-13 has a trigonal space group with unit cell lengths of $a = b = 24.82$ Å and $c = 56.73$ Å.[4] Despite the identical metal oxide and organic linker in IRMOF-13 and IRMOF-14, IRMOF-13 has a catenated framework and differs in the topology from IRMOF-14. The pore diameters in IRMOF-13 are 12.4 and 8.7 Å, smaller than those in IRMOF-14 due to catenation. PCN-6′ is a noncatenated structure with boracite net topology similar to that of Cu-BTC. The primary building block is 4,4′,4″-s-triazine-2,4,6-triyltribenzoate (TATB) instead of benzene-1,3,5-tricarboxylate (BTC) in Cu-BTC. It has a cubic structure with unit cell length of 46.64 Å and a void cuboctahedron with diameter 30.32 Å. The open square pores in PCN-6′ are 15.16 × 15.16 Å^2 or 21.44 × 21.44 Å^2 along the edges or diagonals. PCN-6 is a catenated counterpart of PCN-6′ and can be reproduced by two identical catenated nets of PCN-6′.[38] It exists in the *R*-3*m* space group with cell dimensions of $a = b = 32.97$ Å and $c = 80.78$ Å. PCN-6 contains octahedral cages with edge length of 16 Å and triangular channels of 9.2 Å along the edge. The experimentally determined Langmuir surface area and pore volume are 2700 m^2/g and 1.045 mL/g in PCN-6′, which rise to 3800 m^2/g and 1.453 mL/g in PCN-6. Apparently, catenation leads to an increase of 41% in surface area and of 39% in pore volume.[11]

The interactions between alkanes and MOFs were modeled by LJ potentials. The LJ parameters for MOFs were adopted

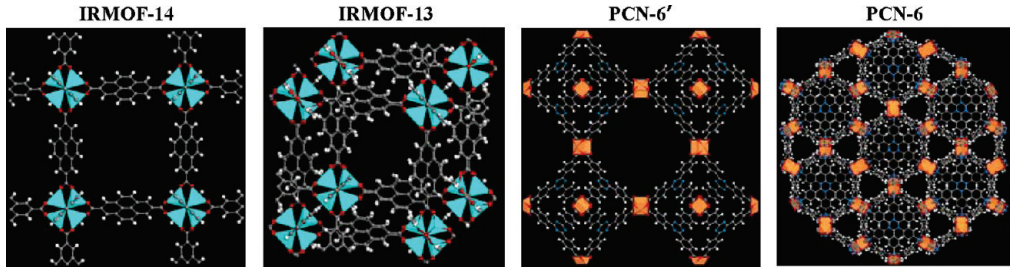

Figure 1. Atomic structures of IRMOF-14, IRMOF-13, PCN-6′, and PCN-6. Zn, cyan polyhedra; Cu, orange polyhedra; O, red; N, blue; C, gray; H, white.

from the universal force field (UFF).[39] The cross LJ parameters were obtained using the Lorentz−Berthelot combining rules. A number of simulation studies have shown that UFF can accurately predict gas adsorption and diffusion in various MOFs. For instance, good agreement between simulation and experiment was obtained for Ar adsorption in Cu-BTC.[40] Simulated isotherms and diffusivities of CO_2 and CH_4 in IRMOF-1 matched well with experimental data.[41,42]

3. Methods

Adsorption of C_4 and C_5 alkane isomer mixtures in the four MOFs was simulated by the grand-canonical MC (GCMC) method at room temperature ($T = 300$ K). The conventional Metropolis techniques in MC simulation are prohibitively expensive in sampling the conformation of alkane molecules. To improve the efficiency, the advanced configurational-bias technique was adopted in which a molecule was grown atom-by-atom, biasing energetically favorable configurations while avoiding overlap with other atoms.[43−45] At first, eight trial positions were generated with a probability proportional to $\exp(-\beta U^i_{\text{internal}})$, where $\beta = 1/k_B T$ and U^i_{internal} are the internal energy at a position i including the intramolecular bond bending and dihedral torsion interactions. Then, one of the trial positions was chosen for growing an atom with a probability proportional to $\exp(-\beta U^i_{\text{external}})/\sum_i \exp(-\beta U^i_{\text{external}})$, where U^i_{external} is the external energy including all nonbonded intramolecular and intermolecular LJ interactions. In addition, the insertion of molecules was enhanced using the multiple first-bead scheme with 15 trial positions.[46]

All the four MOFs were treated as rigid, and the periodic boundary conditions were used in three dimensions to mimic crystalline periodicity. As our study of adsorption was focused on low-energy equilibrium configurations, framework flexibility would not exert a significant effect. A recent simulation study for noble gases and hydrogen in IRMOF-1 showed that there was a negligible difference in adsorption loading between rigid and flexible frameworks.[47] The simulation box contained one unit cell for IRMOF-14 and PCN-6′, and four ($2 \times 2 \times 1$) unit cells for IRMOF-13 and PCN-6. No finite-size effect was found in a larger box with eight ($2 \times 2 \times 2$) unit cells. A spherical cutoff length equal to half of the minimum box length was used to evaluate the LJ interactions with long-range corrections included.

A typical GCMC simulation was carried out for 20000 cycles, in which the first 10000 cycles were used for equilibration and the second 10000 cycles for ensemble averages. Each cycle consisted of a number of trial moves: (a) Translation. A randomly selected adsorbate molecule was translated with a random displacement in either the x, y, or z dimension, and the maximum displacement was adjusted to an overall acceptance ratio of 50%. (b) Rotation. A randomly selected adsorbate molecule was rotated around either the x, y, or z dimension with a random angle, and the maximum angle was adjusted to an overall acceptance ratio of 50%. (c) Partial regrowth. Part of a randomly selected adsorbate molecule was regrown locally. It was decided at random which part of the molecule was regrown and from which bead the regrowth was started. (d) Complete regrowth. A randomly selected adsorbate molecule was regrown completely at a random position. (e) Swap with reservoir. A new adsorbate molecule was created at a random position, or a randomly selected adsorbate molecule was deleted. To ensure microscopic reversibility, the creation and deletion were attempted at random with equal probability. (f) Exchange of molecular identity. An adsorbate molecule was selected randomly and an attempt was made to change its molecular identity. While this trial move is usually not required in GCMC simulation, its use allows reaching equilibrium faster and reduces fluctuations after equilibration.[48] Statistical uncertainty was estimated by the block transformation technique[49] and found to be generally smaller than the symbol sizes presented in the figures. Within statistical uncertainty, the simulation results were independent of the sequence of the trial moves.

Diffusion of C_4 and C_5 alkane isomers was examined using the DL_POLY program.[50] The simulations were carried out in a canonical ensemble at $T = 300$ K. The Nosé−Hoover thermostat was used to maintain temperature with a relaxation constant of 0.8 fs. The equations of motion were integrated using a velocity verlet algorithm, and the time step was 1 fs. Similar to the GCMC simulations, the simulation box for IRMOF-14 and PCN-6′ contained one unit cell, while four ($2 \times 2 \times 1$) unit cells were used for IRMOF-13 and PCN-6. Nevertheless, at low loadings, the simulation box size was increased to eight ($2 \times 2 \times 2$) unit cells in order to accommodate at least 50 molecules to ensure the desired level of statistical accuracy. MOF structures were assumed to be rigid, and the framework atoms were fixed during MD simulation. However, it should be noted that diffusion might be influenced by framework flexibility. For example, diffusion in zeolites is usually accelerated in a flexible model due to the increased possible pathways for the molecular jump.[51] A reduction of diffusion was observed in a flexible carbon nanotube by taking into account the energy exchange between diffusing molecules and a nanotube.[52] The activation energy of benzene in a rigid model of IRMOF-1 was found to be considerably smaller than that in a flexible model, and hence a higher diffusivity was observed in the former.[53] This was attributed to the correlation motion of benzene with the phenylene rings of IRMOF-1, leading to an increase of benzene population in the A-cell pockets.[53] In our MD simulations, the initial configurations were taken from the GCMC simulations mentioned above. The MD simulations were performed for a total period of 5 ns, with the first half left out for equilibration and the second half for the ensemble average.

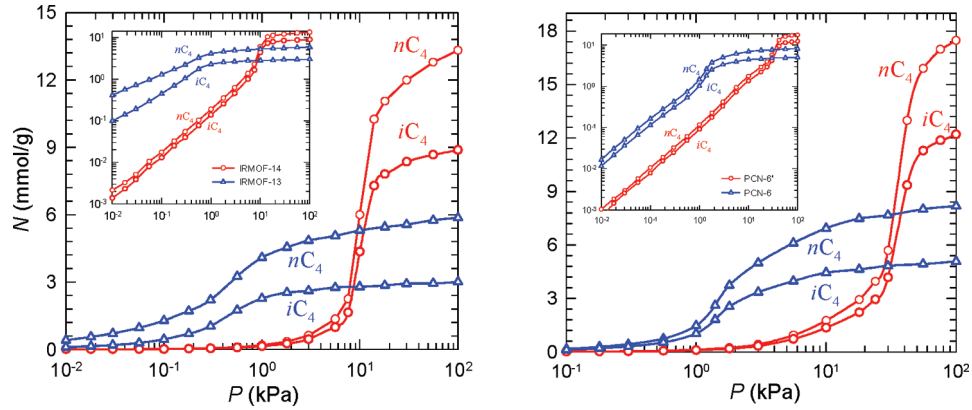

Figure 2. Adsorption isotherms of an nC_4/iC_4 mixture in IRMOF-14, IRMOF-13, PCN-6′, and PCN-6. The insets are in the log−log scale for the clarity of isotherm inflection. The circles are in IRMOF-14 and PCN-6′; the triangles are in IRMOF-13 and PCN-6.

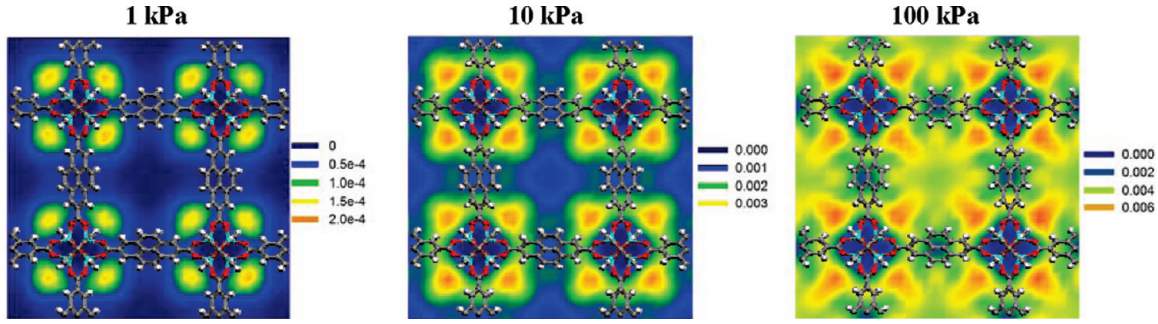

Figure 3. Density contours of the nC_4 isomer in IRMOF-14 at 1, 10, and 100 kPa, respectively. The unit of density is $1/Å^3$.

As we shall see, 2.5 ns was sufficiently long for alkane molecules to reach normal diffusion. During the production run, the atomic coordinates and velocities were written to a disk every 1 ps. The diffusivities were estimated from the mean-squared displacements based on the Einstein relation.[54] Statistical uncertainty was estimated by calculating the standard deviation of diffusivities in different time ranges, e.g., 200−1000 ps, 300−1000 ps, 400−1000 ps, etc. Unless otherwise mentioned, the statistical uncertainty was generally smaller than the symbol sizes presented in the figures.

4. Results and Discussion

4.1. Adsorption. Figure 2 shows the adsorption isotherms of an equimolar mixture of nC_4 and iC_4 isomers in IRMOF-14, IRMOF-13, PCN-6′, and PCN-6, respectively. At low pressures, both isomers have a similar amount of adsorption, particularly, in noncatenated IRMOF-14 and PCN-6′ possessing relatively larger pores. Upon increasing pressure, nC_4 exhibits a greater increase in adsorption than iC_4 and reaches a higher saturation capacity. This implies that a competitive adsorption occurs between nC_4 and iC_4 at high pressures. The packing efficiency in MOFs is better for a linear isomer with a lower degree of branching, in accordance with the concept of shape selectivity; that is, a slender isomer is preferentially adsorbed over a bulky one due to the effect of configurational entropy. As shown in the inset, interestingly, the isotherm exhibits an inflection for both isomers. Note that the inflection may result in steplike adsorption, as observed in our previous study for alkanes in IRMOF-1.[26] Adsorption of nC_4 and iC_4 starts to increase at almost the same pressure, remarkably different from adsorption behavior in MFI zeolite.[55,56] In the latter, iC_4 adsorption reaches a maximum and then decreases due to the small pore size of MFI and the repulsive interaction between adsorbates, whereas nC_4 adsorption increases with increasing pressure until saturation and replaces iC_4.[55,56] Such a trend is not observed here because the pore sizes of the four MOFs are sufficiently larger compared with the critical diameters of C_4 isomers, which enables both linear and branched C_4 isomers to coexist even at high pressures.

Comparing IRMOF-13 and IRMOF-14, the extent of adsorption for both nC_4 and iC_4 in IRMOF-13 is greater at low pressures and the reverse is observed at high pressures. This is due to the presence of constricted pores in IRMOF-13 with a catenated framework. Consequently, adsorbate experiences a stronger potential overlap in IRMOF-13 than in IRMOF-14, leading to a greater adsorption at low pressures. With increasing pressure, however, it becomes difficult to accommodate adsorbate molecules in IRMOF-13 due to its smaller pore volume, particularly, upon saturation. Similar behavior is observed in the adsorption of C_4 isomers in PCN-6 and PCN-6′. Thus, adsorption capacity at low pressures is higher in catenated MOFs than in the noncatenated counterparts, while the opposite is observed at high pressures.

To identify the favorable adsorption sites in the framework, Figure 3 shows the density contours of nC_4 in IRMOF-14 at 1, 10, and 100 kPa. The contours were generated on the basis of the locations of the centers-of-mass of nC_4 molecules during simulation. At a low pressure (1 kPa), adsorption occurs preferentially close to the metal-oxide clusters. This resembles the adsorption of small gases in IRMOF-1 verified both experimentally and theoretically.[57] The corner regions surrounding metal-oxide clusters are small and get saturated quickly; consequently, when pressure increases to 10 kPa, adsorption starts to occur near the organic linkers. At a high pressure (100 kPa), adsorbates are further adsorbed into the open pores. Such sequential adsorption at multiple sites leads to the isotherm inflection observed in Figure 2. The contours of iC_4 are similar; however, its density value at a given pressure is lower than that of nC_4. Figure 4 shows the density contours for nC_4 in IRMOF-

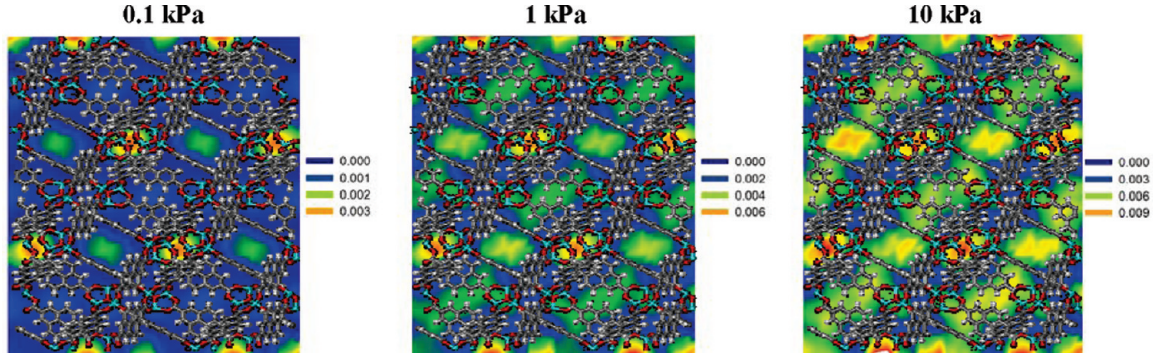

Figure 4. Density contours of the nC_4 isomer in IRMOF-13 at 0.1, 1, and 10 kPa, respectively.

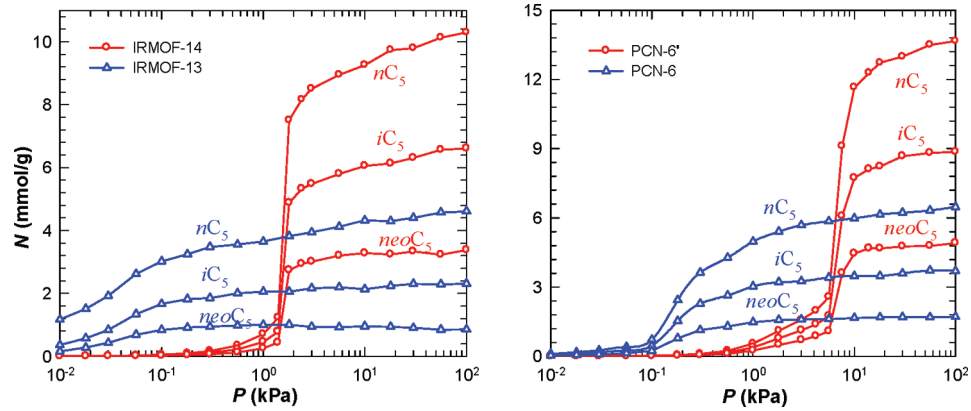

Figure 5. Adsorption isotherms of an $nC_5/iC_5/neoC_5$ mixture in IRMOF-14, IRMOF-13, PCN-6′, and PCN-6. The circles are in IRMOF-14 and PCN-6′; the triangles are in IRMOF-13 and PCN-6.

13. Due to framework catenation, the preferential adsorption sites in IRMOF-13 are the narrow pores constricted between pyrene rings. This is remarkably different from the case of IRMOF-14, in which the corner regions have the strongest binding affinity. With increasing pressure, the constricted pores are progressively filled by adsorbates.

Figure S1 in the Supporting Information shows the density contours of nC_4 in PCN-6′ at 10, 50, and 100 kPa. Similar to the observation in our recent work for the adsorption of CO_2 and CH_4 in Cu-BTC and PCN-6′,[58] at a low pressure (10 kPa), adsorbates are preferentially adsorbed inside octahedral pockets. The pockets are formed by four 4,4′,4″-s-triazine-2,4,6-triyl-tribenzenes. With increasing pressure to 50 kPa, the pockets get saturated and adsorbates enter the windows connecting the pockets. At a high pressure (100 kPa), adsorption further occurs near the exposed metal-sites and organic linkers, and finally in the open pores. This clearly indicates the presence of different adsorption sites in PCN-6′. The linear and branched C_4 isomers have similar locations, but the latter has a lower density. Figure S2 shows the density contours of nC_4 in PCN-6 at different pressures. Similar to the case in PCN-6′, adsorption first occurs in octahedral pockets at a low pressure. With increasing pressure, the constricted triangular pores due to catenation are gradually occupied.

Figure 5 shows the adsorption isotherms of an equimolar $nC_5/iC_5/neoC_5$ mixture in IRMOF-13, IRMOF-14, PCN-6, and PCN-6′. The behavior of the ternary mixture of C_5 isomers resembles that of the nC_4/iC_4 mixture described earlier. At low pressures, the linear and branched C_5 isomers exhibit similar amounts of adsorption. With increasing pressure, the adsorption of each isomer increases, whereas nC_5 increases the most greatly with the highest saturation capacity. At a given pressure, the loading decreases with increased degree of branching due to the configurational entropy effect. Adsorption of both linear and branched C_5 is higher in IRMOF-13 and PCN-6 than in IRMOF-14 and PCN-6′ at low pressures but lower at high pressures. This is a consequence of the presence of narrower pores in catenated IRMOF-13 and PCN-6, and the availability of larger pore volumes to accommodate more adsorbates at high pressures in the noncatenated counterparts. PCN-6′ and PCN-6 show higher saturation capacity than IRMOF-14 and IRMOF-13 because of the larger surface areas and higher free volumes.

In separation processes, the important factor is selectivity among different components. Figure 6 shows the adsorption selectivity of nC_4 over iC_4, nC_5 and iC_5 over $neoC_5$ as a function of pressure. Due to the large pores existing in the four MOFs, the linear and branched isomers can coexist even at high pressures; therefore, the selectivity is not very high. In IRMOF-13 and PCN-6 with constricted pores, the selectivity for both C_4 and C_5 isomer mixtures is generally higher than in the noncatenated counterparts. This implies that adsorptive separation in MOFs could be improved by adjusting the pore size via framework catenation. The selectivity of nC_4/iC_4 in IRMOF-13 decreases as a function of pressure and reaches almost a constant at high pressures; however, it increases slightly in IRMOF-14, PCN-6 and PCN-6′. The decrease of selectivity in IRMOF-13 is due to the reduced interaction between nC_4 and framework upon increasing pressure. The relatively constant selectivity observed in other MOFs is attributed to the large pore size present and consequently the interaction is not significantly affected over the pressure range under study. PCN-6 has a higher saturation loading for C_4 isomers than IRMOF-13; however, the selectivity is lower in PCN-6 especially at low pressures. The higher saturation loading in PCN-6 is simply because of the larger pore volume and surface area, whereas the lower selectivity is due to the existence of pores in PCN-6

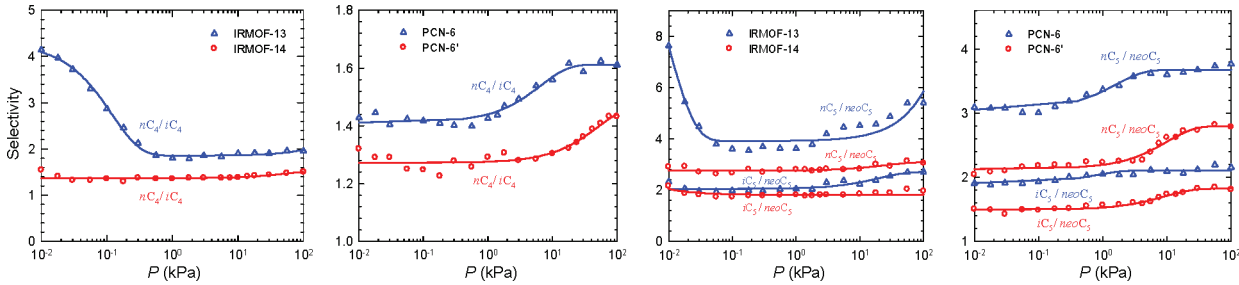

Figure 6. Selectivity of nC4/iC4 and nC5/iC5/*neo*C5 mixtures in IRMOF-14, IRMOF-13, PCN-6′, and PCN-6. The circles are in IRMOF-14 and PCN-6′; the triangles are in IRMOF-13 and PCN-6. The lines are the best fits to the simulation results.

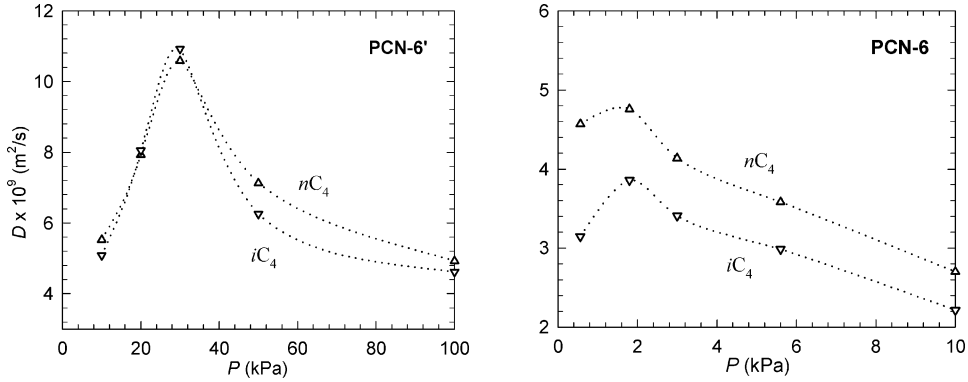

Figure 7. Diffusivities of an nC4/iC4 mixture in PCN-6′ and PCN-6. The dotted lines are for visual clarity.

with size range not well suited for the separation of C_4 isomers as compared with IRMOF-13.

Similarly, the selectivity of nC5 or iC5 with respect to *neo*C5 is higher in catenated MOFs than in the noncatenated counterparts. Interestingly, the selectivity of nC5/*neo*C5 in IRMOF-13 shows a different trend compared with that of nC4/iC4. The selectivity initially decreases at low pressures, reaches a constant at intermediate pressures, and finally increases with pressure. The reason for the initial decrease is similar to that mentioned earlier for C_4 isomers in IRMOF-13. The increase at high pressures occurs because only nC5 continues to be adsorbed beyond a specific pressure (∼1 kPa), whereas *neo*C5 is depleted to some extent (see Figure 5). Again, this is due to the configurational entropy effect, in which the branched isomer is too bulky to intercalate into already packed pores. Nevertheless, the selectivity of nC5/*neo*C5 in IRMOF-14 is nearly a constant. This is because at low pressures the adsorption of both linear and branched C_5 isomers is low and almost the same. With increasing pressure, the degree of increase in adsorption is also similar for both isomers, though the nC5 isomer shows a higher capacity due to the configurational entropy. The selectivity of iC5/*neo*C5 in both IRMOF-13 and IRMOF-14 is approximately equal to 2; nevertheless, the selectivity in IRMOF-13 is slightly larger due to the catenation effect. Compared with that in IRMOF-13, the selectivity of nC5/*neo*C5 in PCN-6 is different, in which case the selectivity remains constant at low pressures and increases slightly with pressure. The increase at high pressures is similar to the observation in IRMOF-13, and such behavior also exists in PCN-6′. In PCN-6 and PCN-6′, the selectivity of iC5/*neo*C5 is about 1.5−2 over the entire range of pressure. The adsorption capacity of C_5 isomer mixtures in MOFs is greater than that in carbon nanotube bundles[22] and silicalite;[20,59] however, the adsorption selectivity is comparable in these different types of materials.

4.2. Diffusion. To investigate the intracrystalline diffusion in noncatenated and catenated MOFs, the diffusivities of C_4 and C_5 isomers in the four MOFs were calculated from MD simulations. Figure S3 of the Supporting Information shows the mean-squared displacements (MSDs) for nC4 and iC4 in PCN-6′. In the log−log scale, MSD increases linearly with time t after 200 ps. That is, MSD is proportional to t^{α} with $\alpha \approx 1$. This reveals that the MD simulation used was sufficiently long for the sorbate molecules to reach normal diffusion. The diffusivities were estimated in the time range from 200 to 1000 ps by the Einstein equation.

Diffusivities of C_4 isomers in IRMOF-14 and IRMOF-13, shown in Figure S4, decrease monotonically as a function of pressure. This behavior is commonly observed and attributed to the increasingly important steric effect with loading, which retards diffusion. Interestingly, the diffusivities of C_4 isomers in PCN-6′ and PCN-6 do not behave in such a way. As shown in Figure 7, the diffusivities initially increase, reach a maximum, and finally decrease with pressure. This type of behavior has been recently observed for the diffusion of C_4 and C_5 alkanes in Cu-BTC,[31] and also in the cage-type zeolites with narrow windows such as LTA, CHA, DDR, and ERI.[60] The initial increase can be interpreted in terms of a reduction in the free energy barrier for intercage hopping. More specifically, at a low pressure, adsorbates in PCN-6′ are preferentially located inside the octahedral pocket, as illustrated in Figure S1. The pocket has a limited space, and hence, the diffusion is largely prohibited. As pressure increases, however, adsorbates populate near the open metal-sites and further in the large open pores; consequently, diffusivity increases until a maximum. With further increasing pressure, the diffusivities decrease simply due to steric hindrance.

The diffusivities of nC4 and iC4 in PCN-6 also initially increase and then decrease with increasing pressure. Similar to the case of PCN-6′, at a low pressure, adsorbates are located in the octahedral pockets; therefore, diffusivity is small in the limited space. With increasing pressure, nC4 and iC4 can diffuse from the pockets to the triangular pores and, hence, the diffusivity increases. Nevertheless, the increase in PCN-6 is not so sharp as in PCN-6′ due to the framework catenation in PCN-

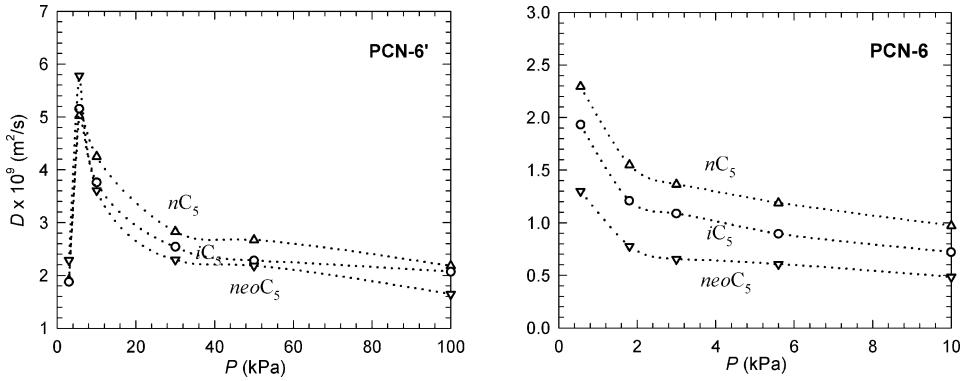

Figure 8. Diffusivities of an $nC_5/iC_5/neoC_5$ mixture in PCN-6′ and PCN-6. The dotted lines are for visual clarity.

6, which leads to a higher free energy barrier for hopping. In addition, as expected, the diffusivity magnitude in PCN-6 is smaller than that in PCN-6′. Comparing nC_4 and iC_4 isomers, in general, nC_4 diffuses faster than iC_4 in both structures. This is because nC_4 has a slender shape and can more easily diffuse through narrow regions than iC_4. Interestingly, the diffusivity difference between the two isomers in PCN-6 is larger than that in PCN-6′, particularly at low pressures. In other words, diffusion selectivity is enhanced by catenation, which has not been reported before in the literature.

Figure 8 shows the diffusivities of a C_5 isomer mixture in PCN-6′ and PCN-6 as a function of pressure. In PCN-6′, the diffusion characteristics of C_5 isomers resemble those of C_4 isomers, even though the diffusivity values of the former are smaller. Except at very low pressures in PCN-6′, the diffusivities follow the order of $nC_5 > iC_5 > neoC_5$, consistent with the increased degree of branching. That is, a more slender isomer diffuses faster than a bulky one. In PCN-6, the diffusivities drop monotonically with increasing pressure, in contrast to the case of C_4 isomers. While C_4 isomers can diffuse relatively easily in narrow triangular channels of PCN-6, diffusion of C_5 isomers is retarded because of their bulky sizes and also their stronger interactions with the framework compared with the case of C_4 isomers. Consequently, C_5 isomers show a decrease in diffusivity as a function of pressure. The diffusion characteristics of a C_5 isomer mixture in PCN-6 are similar to those observed for an nC_6/iC_6 mixture in MFI,[21] a CH_4/CO_2 mixture in silicalite,[42,61] and C_1/C_2, C_1/C_3, and C_1/nC_4 mixtures in carbon nanotubes,[62] where diffusivities also decrease monotonically due to the steric hindrance. In general, the diffusivities of C_4 or C_5 isomers in PCN-6 are smaller than those in PCN-6′. However, the diffusion selectivity among isomers is larger in catenated PCN-6. Movies are provided in the Supporting Information for the diffusion of C_5 isomers in PCN-6′ and PCN-6, respectively, in which the diffusion pathway is shown.

In separation processes, the efficacy is characterized by permselectivity, which depends on adsorption selectivity—an equilibrium property—and diffusion selectivity—a dynamic property. As shown in Figure 6, a linear isomer has a stronger adsorption over a branched isomer. Figures S4, 7, and 8 further demonstrate that a linear isomer diffuses faster. Combining these two factors, a linear isomer has a larger permeability than its branched counterpart, and a mixture of isomers can be separated. Moreover, both adsorption and diffusion selectivities are found to be larger in catenated IRMOF-13 and PCN-6 than in noncatenated IRMOF-14 and PCN-6′. This suggests that framework catenation might be an appropriate way to enhance separation efficacy.

5. Conclusions

Adsorption and diffusion of alkane (C_4 and C_5) isomer mixtures in IRMOF-13, IRMOF-14, PCN-6, and PCN-6′ have been investigated using molecular simulations. The isotherms show a linear isomer has a larger loading than the branched one because the configurational entropy effect favors the packing of the linear isomer. Due to catenation, IRMOF-13 and PCN-6 have a stronger adsorption for both linear and branched isomers at low pressures compared with noncatenated IRMOF-14 and PCN-6′. However, the reverse is observed at high pressures due to the smaller pore volume in catenated MOFs. The preferential adsorption sites in IRMOF-14 are near the metal-oxides, in contrast to the constricted pores in IRMOF-13. In PCN-6′, adsorption occurs first in the octahedral pockets, then near the metal-sites and organic linkers, and finally in the open pores. In PCN-6, adsorption first occurs in the octahedral pockets and then in the constricted triangular pores. The sequential adsorption leads to inflection observed in the isotherms. IRMOF-13 exhibits the highest adsorption selectivity for C_4 and C_5 isomer mixtures in the four MOFs studied. Compared with a carbon nanotube bundle and silicalite, MOFs exhibit greater adsorption capacity and comparable adsorption selectivity.

The diffusivities of alkane isomers in IRMOF-13, IRMOF-14, PCN-6, and PCN-6′ decrease in the order of $nC_4 > iC_4$ and $nC_5 > iC_5 > neoC_5$ because a slender molecule can diffuse faster than a bulky one. In IRMOF-14 and IRMOF-13, the diffusivities decrease with pressure simply due to the steric effect. Nevertheless, the diffusivities in PCN-6′ initially increase with pressure, pass a maximum, and finally decrease. The reason is that at low pressures adsorbates in PCN-6′ are preferentially located in the octahedral pockets and thus the diffusion is largely prohibited. As pressure increases, however, adsorbates start to reside near the metal-sites and in the center pores; consequently, the diffusivities increase in the relatively large open space. Finally, the decrease is attributed to the steric hindrance at high pressures. While C_4 isomers exhibit a similar trend of diffusivity in PCN-6 and PCN-6′, C_5 isomers in PCN-6 behave differently from those in PCN-6′ with monotonically decreasing diffusivity. This is primarily due to the steric effect of bulky C_5 isomers. The diffusivities in IRMOF-13 and PCN-6 are smaller than those in IRMOF-14 and PCN-6′ because catenation leads to a higher free energy barrier for hopping and also many open sites are blocked. Remarkably, both adsorption and diffusion selectivities are enhanced in catenated IRMOF-13 and PCN-6, implying that separation efficacy can be improved by catenation.

Acknowledgment. The authors gratefully acknowledge the National University of Singapore for funding.

Supporting Information Available: Density contours of nC_4 in PCN-6′ and PCN-6. Mean-squared displacements of nC_4 and iC_4 in PCN-6′. Diffusivities of nC_4/iC_4 mixture in IRMOF-14 and IRMOF-13. Movies for the diffusion of C_5 isomers in PCN-6′ and PCN-6. This material is available free of charge via the Internet at http://pubs.acs.org.

References and Notes

(1) Yaghi, O. M.; O'Keeffe, M.; Ockwig, N. W.; Chae, H. K.; Eddaoudi, M.; Kim, J. *Nature* **2003**, *423*, 705.
(2) Koh, K.; Wong-Foy, A. G.; Matzger, A. J. *J. Am. Chem. Soc.* **2009**, *131*, 4184.
(3) Rowsell, J. L. C.; Yaghi, O. M. *Microporous Mesoporous Mater.* **2004**, *73*, 3.
(4) Eddaoudi, M.; Kim, J.; Rosi, N.; Vodak, D.; Wachter, J.; O'Keefe, M.; Yaghi, O. M. *Science* **2002**, *295*, 469.
(5) Millward, A. R.; Yaghi, O. M. *J. Am. Chem. Soc.* **2005**, *127*, 17998.
(6) Düren, T.; Sarkisov, L.; Yaghi, O. M.; Snurr, R. Q. *Langmuir* **2004**, *20*, 2683.
(7) Yang, Q. Y.; Zhong, C. L.; Chen, J. F. *J. Phys. Chem. C* **2008**, *112*, 1562.
(8) Babarao, R.; Jiang, J. W. *Langmuir* **2008**, *24*, 6270.
(9) Bae, Y. S.; Mulfort, L. K.; Frost, H.; Ryan, P.; Punnathanam, S.; Broadbelt, L. J.; Hupp, J. T.; Snurr, R. Q. *Langmuir* **2008**, *24*, 8592.
(10) Jung, D. H.; Kim, D.; Lee, T. B.; Choi, S. B.; Yoon, J. H.; Kim, J.; Choi, K.; Choi, S. H. *J. Phys. Chem. B* **2006**, *110*, 22987.
(11) Ma, S. Q.; Sun, D. F.; Ambrogio, M.; Fillinger, J. A.; Parkin, S.; Zhou, H. C. *J. Am. Chem. Soc.* **2007**, *129*, 1858.
(12) Chen, B. L.; Ma, S. Q.; Hurtado, E. J.; Lobkovsky, E. B.; Zhou, H. C. *Inorg. Chem.* **2007**, *46*, 8490.
(13) Liu, B.; Yang, Q. Y.; Xu, C. H.; Zhong, C. L.; Chen, B.; Smit, B. *J. Phys. Chem. C* **2008**, *112*, 9854.
(14) Denayer, J. F.; Souverijns, W.; Jacobs, P. A.; Martens, J. A.; Baron, G. V. *J. Phys. Chem. B* **1998**, *102*, 4588.
(15) Savitz, S.; Siperstein, F.; Gorte, R. J.; Myers, A. L. *J. Phys. Chem. B* **1998**, *102*, 6865.
(16) Hernandez, M. A.; Velasco, J. A.; Asomoza, M.; Solis, S.; Rojas, F.; Lara, V. H.; Portillo, R.; Salgado, M. A. *Energy Fuels* **2003**, *17*, 262.
(17) Smit, B.; Siepmann, J. I. *Science* **1994**, *264*, 1118.
(18) Maginn, E. J.; Bell, A. T.; Theodorou, D. N. *J. Phys. Chem.* **1995**, *99*, 2057.
(19) Maris, T.; Vlugt, T. J. H.; Smit, B. *J. Phys. Chem. B* **1998**, *102*, 7183.
(20) Calero, S.; Smit, B.; Krishna, R. *Phys. Chem. Chem. Phys.* **2001**, *3*, 4390.
(21) Krishna, R.; Smit, B.; Calero, S. *Chem. Soc. Rev* **2002**, *31*, 185.
(22) Jiang, J. W.; Sandler, S. I.; Schenk, M.; Smit, B. *Phys. Rev. B* **2005**, *72*, 045447.
(23) Jiang, J. W.; Sandler, S. I. *J. Chem. Phys.* **2006**, *124*, 024717.
(24) Jiang, J. W. *J. Phys. Chem. B* **2006**, *110*, 8670.
(25) Düren, T.; Snurr, R. Q. *J. Phys. Chem. B* **2004**, *108*, 15703.
(26) Jiang, J. W.; Sandler, S. I. *Langmuir* **2006**, *22*, 5702.
(27) Barcia, P. S.; Zapata, F.; Silva, J. A. C.; Rodrigues, A. E.; Chen, B. L. *J. Phys. Chem. B* **2007**, *111*, 6101.
(28) Chen, B. L.; Liang, C. D.; Yang, J.; Contreras, D. S.; Clancy, Y. L.; Lobkovsky, E. B.; Yaghi, O. M.; Dai, S. *Angew. Chem. Int. Ed.* **2006**, *45*, 1390.
(29) Li, K. H.; Lee, J. Y.; Olson, D. H.; Emge, T. J.; Bi, W. H.; Eibling, M. J.; Li, J. *Chem. Commun.* **2008**, *46*, 6123.
(30) Dubbeldam, D.; Galvin, C. J.; Walton, K. S.; Ellis, D. E.; Snurr, R. Q. *J. Am. Chem. Soc.* **2008**, *130*, 10884.
(31) Chmelik, C.; Karger, J.; Wiebckw, M.; Caro, J.; van Baten, J. M.; Krishna, R. *Microporous Mesoporous Mater.* **2009**, *117*, 22.
(32) Ryckaert, J. P.; Bellemans, A. *Faraday Discuss. Chem. Soc.* **1978**, *66*, 95.
(33) Macedonia, M. D.; Maginn, E. J. *Fluid Phase Equilib.* **1999**, *158*−*160*, 19.
(34) Martin, M. G.; Siepmann, J. I. *J. Phys. Chem. B* **1998**, *102*, 2569.
(35) Martin, M. G.; Siepmann, J. I. *J. Phys. Chem. B* **1999**, *103*, 4508.
(36) Klauda, J. B.; Brooks, B. R.; MacKerell, A. D.; Venable, R. M.; Pastor, R. W. *J. Phys. Chem. B* **2005**, *109*, 5300.
(37) Klauda, J. B.; Pastor, R. W.; Brooks, B. R. *J. Phys. Chem. B* **2005**, *109*, 15684.
(38) Sun, D. F.; Ma, S. Q.; Ke, Y. X.; Collins, D. J.; Zhou, H. C. *J. Am. Chem. Soc.* **2006**, *128*, 3896.
(39) Rappe, A. K.; Casewit, C. J.; Colwell, K. S.; Goddard, W. A.; Skiff, W. M. *J. Am. Chem. Soc.* **1992**, *114*, 10024.
(40) Vishnyakov, A.; Ravikovitch, P. I.; Neimark, A. V.; Bulow, M.; Wang, Q. M. *Nano Lett.* **2003**, *3*, 713.
(41) Babarao, R.; Hu, Z. Q.; Jiang, J. W.; Chempath, S.; Sandler, S. I. *Langmuir* **2007**, *23*, 659.
(42) Babarao, R.; Jiang, J. W. *Langmuir* **2008**, *24*, 5474.
(43) Siepmann, J. I.; Frenkel, D. *Mol. Phys.* **1992**, *75*, 59.
(44) Frenkel, D.; Mooij, G. C. A. M.; Smit, B. *J. Phys.: Condensed Matter* **1992**, *4*, 3053.
(45) de Pablo, J. J.; Laso, M.; Suter, U. W. *J. Chem. Phys.* **1992**, *96*, 2395.
(46) Esselink, K.; Loyens, L. D. J. C.; Smit, B. *Phys. Rev. E* **1995**, *51*, 1560.
(47) Greathouse, J. A.; Kinnibrugh, T. L.; Allendorf, M. D. *Ind. Eng. Chem. Res.* **2009**, *48*, 3425.
(48) Kofke, D. *Mol. Simul.* **1991**, *7*, 285.
(49) Frenkel, D.; Smit, B. *Understanding Molecular Simulations: From Algorithms to Applications*, 2nd ed.; Academic Press: San Diego, 2002.
(50) Smith, W.; Forester, T. R. *J. Mol. Graph.* **1996**, *14*, 136.
(51) Leroy, F.; Rooousseau, B.; Fuchs, A. H. *Phys. Chem. Chem. Phys.* **2004**, *6*, 775.
(52) Chen, H. B.; Johnson, J. K.; Sholl, D. S. *J. Phys. Chem. B* **2006**, *110*, 1971.
(53) Amirjalayer, S.; Tafipolsky, M.; Schmid, R. *Angew. Chem., Int. Ed.* **2007**, *46*, 463.
(54) Allen, M. P.; Tildesley, D. J. *Computer Simulation of Liquids*; Clarendon Press: Oxford, 1987.
(55) Krishna, R.; Smit, B.; Vlugt, T. J. H. *J. Phys. Chem. A* **1998**, *102*, 7727.
(56) Krishna, R.; Calero, S.; Smit, B. *Chem. Eng. J.* **2002**, *88*, 81.
(57) Dubbeldam, D.; Frost, H.; Walton, K. S.; Snurr, R. Q. *Fluid Phase Equilib.* **2007**, *261*, 152.
(58) Babarao, R.; Jiang, J. W.; Sandler, S. I. *Langmuir* **2009**, *25*, 5239.
(59) Smit, B.; Krishna, R. *Chem. Eng. Sci.* **2003**, *58*, 557.
(60) Krishna, R.; van Baten, J. M. *Microporous Mesoporous Mater.* **2008**, *109*, 91.
(61) Krishna, R.; van Baten, J. M.; Garcia-Perez, E.; Calero, S. *Chem. Phys. Lett.* **2006**, *429*, 219.
(62) Krishna, R.; van Baten, J. M. *Ind. Eng. Chem. Res.* **2006**, *45*, 2084.

JP902253P